PERGAMON

Chaos, Solitons and Fractals 11 (2000) 2129–2140

CHAOS
SOLITONS & FRACTALS

www.elsevier.nl/locate/chaos

A symplectic mapping for the ergodic magnetic limiter and its dynamical analysis

K. Ullmann [*,1], I.L. Caldas

Instituto de Física da Universidade de São Paulo, C.P. 66318, 05315-970 São Paulo, Brazil

Accepted 27 July 1999

Abstract

A model for a new bidimensional sympletic mapping describing magnetic field line trajectories in a tokamak perturbed by ergodic magnetic limiter coils is presented. Numerical examples of these trajectories, computed for plasma described by large aspect-ratio equilibria, simulate the main characteristics of trajectories in the toroidal geometry. Also the importance of the symplecticity of the new mapping regarding certain features of non-linear dynamical analysis, for which a large number of iterations is necessary, is shown. Thus, some standard algorithms, such as the Lyapunov exponents and the rotational transforms, are applied with precision in order to characterize regular and chaotic regions in the parameter space, improving the study of bifurcations, routes to chaos, and diffusion in this system. © 2000 Elsevier Science Ltd. All rights reserved.

1. Introduction

Tokamaks have presented the best performance as magnetic confinement devices for fusion applications. However, for the necessary improvement in the performance of these machines, some technical difficulties have to be solved. In particular, the presence of impurities in the plasma should be reduced to improve the plasma confinement [1,2]. The common sources of such impurities in tokamak plasmas are the heat and particle loadings on the metallic chamber inner wall, causing impurity release by sputtering processes. To avoid this problem, a cold boundary layer, induced by chaotic magnetic field lines, has been used as a plasma limiter, since it uniformizes these loadings, lowering the impurity levels within the plasma core [3,4].

The concept of an ergodic magnetic limiter was introduced in the late 1970s [5,6] and is based on the idea that a chaotic boundary layer of field lines could appear as a result of resonant magnetic disturbing fields perturbing the equilibrium magnetic fields which contain the plasma. This magnetic ergodic limiter consists of a grid-shaped coil wound around the tokamak vessel and conducting a current, generating these disturbing fields [3,7].

This quite complex phenomenon can be well described by maps because the equation of the equilibrium field lines ($\vec{B} \times \mathrm{d}\vec{l} = 0$) outside the influence region of the ergodic magnetic limiter can be analytically integrated, with some minor approximations, and so we deal with a quasi-integrable system, once we consider the influence region of the limiter coils narrow enough, which is a good approximation as shown in [8].

Considering the tokmak as a toroidal chamber with major radius R_0 and minor radius b (Fig. 1) we study the magnetic field line evolution analyzing a Poincaré section which consists of a straight cut of the tokamak vessel at the center of the ergodic magnetic limiter. The points where the field line cuts this

* Corresponding author.
E-mail addresses: kai@if.usp.br (K. Ullmann), ibere@if.usp.br (I.L. Caldas).
[1] Present address: Department of Electrical Engineering and Computer Science, University of California, Berkeley, CA 94720, USA.

0960-0779/00/$ - see front matter © 2000 Elsevier Science Ltd. All rights reserved.
PII: S0960-0779(99)00138-1

Poincaré section are given in polar coordinates (r, θ) with their origin located at the minor tokamak axis. Numerical trajectories are computed considering a large aspect-ratio approximation ($R_0/b \gg 1$) for the plasma equilibrium. Even so, these trajectories simulate quite well the main characteristics of those computed in exact toroidal geometry, as the poloidal asymmetry of the KAM magnetic surfaces and the typical rotational transform radial profiles observed in experiments [2].

Thus, the system considered in this work describes an experimental phenomenon which can be studied with the aid of a mapping. In fact, low-dimensional mappings have been much used for studying non-linear phenomena, such as sensibility to initial conditions and routes to chaos [9,10], in different experimental systems.

However, the study of non-linear phenomena in the system considered in this work, as well as in other conservative systems, may require a large number of iterations for the convergence of the Lyapunov exponents and rotational transforms. Therefore, in order to compute these algorithms with precision, we introduce in this work a symplectic mapping to compute the Poincaré sections of the analyzed field line trajectories. Furthermore, by applying this mapping, we characterize the regular and chaotic regions in our system and present results concerning the bifurcations and transition to chaos, in terms of relevant experimental control parameters and significative initial condition sets.

Numerical examples are presented for typical parameters from the TBR-1 tokamak [8]. However, the main conclusions obtained from these results can easily be extended to other tokamaks since all these machines operate within the same relevant control parameter range used in the present analysis.

This paper is organized as follows: in Section 2 we study the previously existent models of the ergodic magnetic limiter. In Section 3 we introduce our symplectic model for the mapping of the field line trajectories. Then we perform the dynamical analysis of the field lines generated by our model, computing Lyapunov exponents and rotational transforms [11,12] in Section 4. Section 5 is devoted to the analysis of the model with varying initial conditions and parameters. Our conclusions are presented in Section 6.

2. The previous models

One of the first models describing the magnetic field line evolution in a tokamak vessel perturbed by ergodic magnetic limiter coils is the Martin–Taylor mapping [13–15], which consists of two consecutive bidimensional mappings. The first mapping describes the evolution of the magnetic field line along the tokamak vessel (equilibrium field) and is given by:

$$x_n^* = x_n + s y_n, \tag{1a}$$

$$y_n^* = y_n, \tag{1b}$$

where (x_n, y_n) are the rectangular coordinates of the initial position of the field line in the Poincaré plot, (x_n^*, y_n^*) the rectangular coordinates of the final position, and

$$s = -\frac{2\pi b}{q^2}\frac{\mathrm{d}q}{\mathrm{d}y}$$

is the strength of the shear of the equilibrium field (b is the minor tokamak radius and $q(y)$ the safety factor profile, which is related to the rotational transform ι by $q = 2\pi/\iota$).

The second mapping describes the field line evolution in the region of the diffuser grid of 'wavelength' $2\pi b/m$ with a current I in each wire of length l, and is given by

$$x_{n+1} = x_n^* - p\mathrm{e}^{-y_n^*}\cos x_n^*, \tag{2a}$$

$$y_{n+1} = y_n^* + \ln(\cos(x_n^* - p\mathrm{e}^{-y_n^*}\cos x_n^*)) - \ln(\cos x_n^*), \tag{2b}$$

where $p = \pi m^2 lI/b^2 B_0$ measures the strength of the diffuser relative to the toroidal field (B_0 is the intensity of the toroidal field, that is, the magnetic field component along the tokamak camera). In most cases where this mapping was analyzed the magnetic shear $\mathrm{d}q/\mathrm{d}y$ was considered as being constant in the studied

region, and in this case the mapping depends only on two dimensionless parameters p and s. It is also important to observe that, as both cosecutive mappings have unitary Jacobians

$$\left(\frac{\partial(x_n^*, y_n^*)}{\partial(x_n, y_n)} = \frac{\partial(x_{n+1}, y_{n+1})}{\partial(x_n^*, y_n^*)} = 1\right),$$

the whole mapping is area-preserving, and can be described in a Hamiltonian formulation.

Using this mapping to plot a Poincaré section with constant parameters p and s (Fig. 2), we observe the typical island chain structure with chaotic regions around the destroyed separatrixes and secondary island chains around the main islands [16,17]. Although this model describes very well the qualitative behavior of the magnetic field line trajectories, it has some constraints, being the most important of them the total neglect of toroidal effects, which are important in many tokamaks [18].

In order to include toroidal corrections, Viana and Caldas proposed a different model for a mapping of the magnetic field lines in a tokamak under the influence of ergodic magnetic limiter coils [14]. It consists again of two consecutive mappings: one describing the evolution of the equilibrium field lines, and the other the influence of the perturbation introduced by the ergodic magnetic limiter coils. In this case the perturbative field is considered as being modulated by a delta-peak in the toroidal direction. This approximation may seem rather crude but comparisons with numerical integration over step-function models have shown that it leads to very good results [8].

The mapping describing the equilibrium field line evolution along the chamber is given by:

$$r_n^* = r_n, \tag{3a}$$

$$\theta_n^* = \theta_n + \frac{2\pi B_\theta(r_n) R_0}{r_n B_0}, \tag{3b}$$

in the cylindrical case, and introducing a usual approximation of the toroidal field correction in order to take into account the equilibrium poloidal asymmetry

$$B_\phi = \frac{B_0}{1 - \frac{r}{R_0}\cos\theta} \tag{4}$$

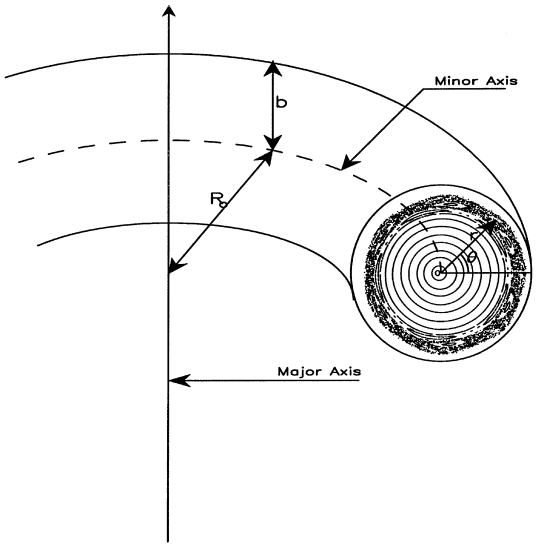

1

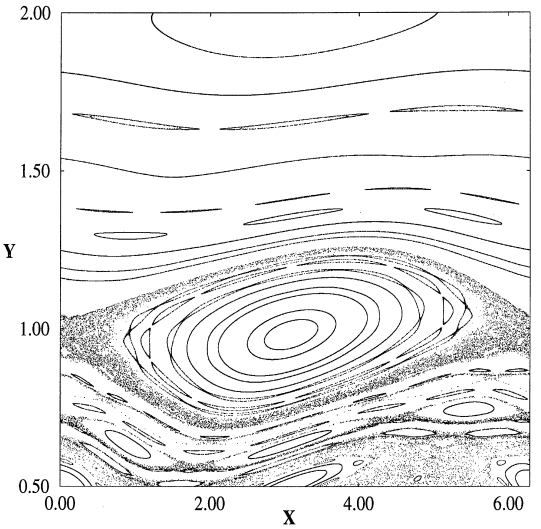

2

Fig. 1. Essential tokamak geometry.

Fig. 2. Martin–Taylor mapping with $p = 0.30$ and $s = 2\pi$.

we obtain the new angular equation with toroidal corrections

$$\theta_n^* = 2\ \arctan(\lambda(r_n)\tan(\Omega(r_n) + \arctan\Xi(r_n,\theta_n))) + 2\pi, \tag{5}$$

where R_0 is the major tokamak radius and $B_\theta(r)$ is the poloidal magnetic field profile, which is related to the safety factor by $B_\theta(r) = B_0 r/R_0 q(r)$. In order to describe the toroidal effects in (5) there were also defined some dimensionless variables:

$$\epsilon(r_n) \equiv \frac{r}{R_0}, \tag{6a}$$

$$\lambda(r_n) \equiv \frac{1-\epsilon(r_n)}{\sqrt{1-\epsilon^2(r_n)}}, \tag{6b}$$

$$\Omega(r_n) \equiv \frac{\pi R_0 B_\theta(r_n)(1-\epsilon(r_n))}{B_0 r_n \lambda(r_n)}, \tag{6c}$$

$$\Xi(r_n,\theta_n) \equiv \lambda(r_n)\tan\left(\frac{\theta_n}{2}\right). \tag{6d}$$

The impulsive action of the ergodic magnetic limiter on the field lines described by the mapping:

$$r_{n+1} = r_n^* - bC\left(\frac{r_n^*}{b}\right)^{m-1}\sin(m\theta_n^*), \tag{7a}$$

$$\theta_{n+1} = \theta_n^* - C\left(\frac{r_n^*}{b}\right)^{m-2}\cos(m\theta_n^*), \tag{7b}$$

where we define the dimensionless constant $C \equiv \mu_0 mIl/B_0\pi b^2$. Plotting Poincaré sections of this mapping, using the TBR-1 parameters (the main parameters are: $R_0 = 0.30m$ (major radius), $b = 0.11m$ (minor radius), $a = 0.08m$ (plasma radius), $B_0 = 0.50T$ (toroidal field at magnetic axis), $q(a) = 5$ (safety factor at plasma edge) and $q(0) = 1$ (safety factor at plasma core)) [19], and using a well-known empirical model for the radial profile of the poloidal magnetic filed

$$B_\theta(r) = \begin{cases} (aB_\theta(a)/r)(1-(1-r^2/a^2)^{\gamma+1}) & (0 < r < a), \\ aB_\theta(a)/r & (a < r < b), \end{cases} \tag{8}$$

(Fig. 3) we observe that for low limiter currents (Fig. 4a) the island chains and the general structure of the Poincaré plot are well described. But as we increase the limiter current (Fig. 4b) the small dissipative effects become more important and although there are large regions of irregular field lines, for small values for y, these are not chaotic but are attracted to some island chain by the dissipative effects sooner or later. This also results in more magnetic island destruction than expected, and so this model, although adequate for the study of magnetic island chains at low limiter currents, cannot be used for the study at higher currents and the dynamical analysis of chaotic field lines.

3. The symplectic model

In order to perform a more accurate study of the onset of chaotic field lines at the tokamak border, we need to develop a field line mapping which can be related directly to the parameters of a given tokamak and is still symplectic [20]. As in the previous models, we split our mapping for the Poincaré section immediately following the ergodic limiter perturbation in two consecutive ones: the first describing the equilibrium field

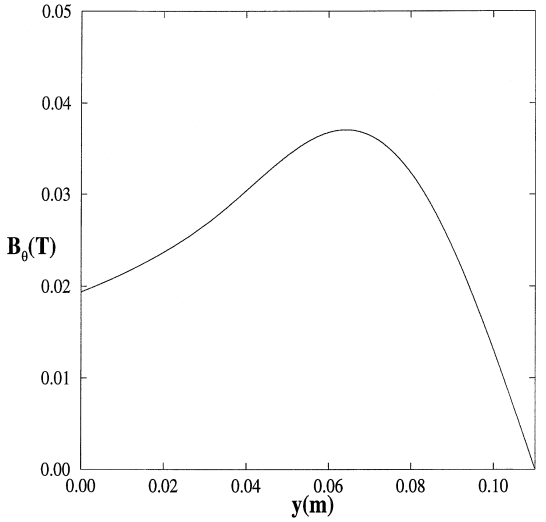

Fig. 3. Radial profile of the poloidal field B_θ with TBR-1 parameters.

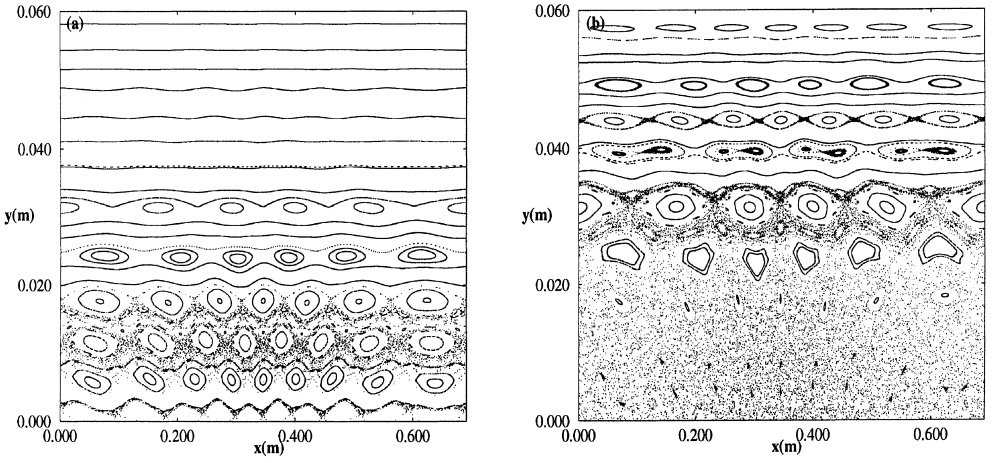

Fig. 4. Poincaré sections of the Viana–Caldas mapping with $m = 6$ and (a) $I = 220$ A, (b) $I = 800$ A in rectangular coordinates $(x = b\theta, y = b - r)$.

line trajectory along the tokamak chamber ($T^1 : (r_n, \theta_n) \to (r_n^*, \theta_n^*)$) and the second describing the effects of the current coils of the ergodic limiter ($T^2 : (r_n^*, \theta_n^*) \to (r_{n+1}, \theta_{n+1})$).

In the cylindrical approximation the equilibrium part of the Viana–Caldas mapping is already symplectic and so we retain it without changes. But we need to introduce a mapping with toroidal corrections that obeys the following conditions:

(a) in the limit $\epsilon = r/R_0 \to 0$ it is reduced to the cylindrical mapping;

(b) the new safety factor profile $q(r)$ must be as similar as possible to the profile of the Viana–Caldas mapping, which describes very well the position of the magnetic island chains and their width at low limiter currents;

(c) it must be obtainable from a generating function, which guarantees its symplecticity [20].

The most generic generating function which insures the properties (a) and (c) above is given by

$$G^1(\epsilon_n^*, \theta_n) = \theta_n \epsilon_n^* + 2\pi J(\epsilon_n^*) + \sum_{l=1}^{\infty} a_l \epsilon_n^{*l} \cos^l \theta_n, \tag{9}$$

where we define the normalized radial coordinate $\epsilon \equiv r/R_0$ and the integral of the inverse safety factor

$$J(\epsilon) = \int_0^{\epsilon} \frac{\mathrm{d}x}{q(x)}.$$

The next step is to fit the arbitrary constants a_l in order to fulfill condition (b). As a matter of fact we verified that a very good profile agreement can be obtained retaining only the first term of the sum with $a_1 = -0.04$ (Fig. 5a). Using the definition of this generating function ($\epsilon_n \equiv \partial G^1/\partial\theta_n$ and $\theta_n^* \equiv \partial G^1/\partial\epsilon_n^*$) we obtain equilibrium mapping equations:

$$r_n^* = \frac{r_n}{1 - a_1 \sin\theta_n}, \tag{10}$$

$$\theta_n^* = \theta_n + \frac{2\pi}{q(r_n^*)} + a_1 \cos\theta_n. \tag{11}$$

Plotting the equilibrium curves obtained by this new equilibrium mapping near the center of the tokamak vessel (Fig. 5b), we observe the poloidal asymmetry of the unperturbed field. Moreover, the magnetic axis and the geometric axis are no longer coincident, as in the Viana–Caldas mapping, but there is a displacement between them. This displacement is known in the literature as the Shafranov shift [18,21] and is well known from numerical solutions of the Grad–Shafranov equation. As in this work we are mainly concerned about the plasma border we did not try to adjust the magnitude of the Shafranov shift to known values, which could have been done by varying a_1 or using further expansion terms.

In order to obtain a symplectic mapping for the action of the ergodic limiter coils, we retain the angular part

$$\theta_{n+1} = \theta_n^* - C\left(\frac{r_n^*}{b}\right)^{m-2} \cos(m\theta_n^*), \tag{12}$$

where we use again the dimensionless constant $C = \mu_0 m I\psi/\pi b^2 B_0$, and using $\theta_{n+1} \equiv \partial G^2/\partial r_{n+1}$ we obtain the generating function

$$G^2(r_{n+1}, \theta_n^*) = r_{n+1}\theta_n^* - \frac{Cb}{m-1}\left(\frac{r_{n+1}}{b}\right)^{m-1} \cos(m\theta_n^*), \tag{13}$$

which leads us to the new radial equations given by

$$r_n^* \equiv \frac{\partial G^2}{\partial \theta_n^*} = r_{n+1} + \frac{mCb}{m-1}\left(\frac{r_{n+1}}{b}\right)^{m-1} \sin(m\theta_n^*). \tag{14}$$

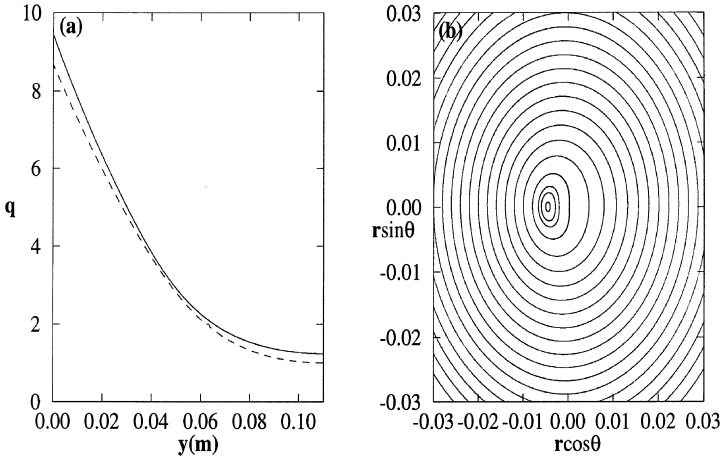

Fig. 5. (a) Safety factor profiles for the Viana–Caldas mapping (solid line) and the symplectic mapping (dashed line); (b) Poincaré plot of the symplectic equilibrium mapping with toroidal corrections.

Plotting a Poincaré section with this symplectic mapping at low limiter current ($I = 200$ A) and using the TBR-1 parameters (Fig. 6a) we can see that the magnetic island chains at the tokamak chamber edge remain very similar to the ones observed in the dissipative Viana–Caldas model (Fig. 4a) both in their radial position and in their island width. They are only more curved due to the effects of the more realistic toroidal corrections. But as we increase the limiter current to $I = 800$ A the differences between the Poincaré plots are relevant: while in the Viana–Caldas model the structure is destroyed by the small dissipative effects, and so no further dynamical analysis is possible (Fig. 4b), in the symplectic mapping the island structure with all its details and the onset of global chaos can be observed very precisely (Fig. 6b), and magnifications of small regions show the typical structure of generic Hamiltonian systems (Fig. 7).

4. The dynamical analysis of field lines

One of the most important methods of analysis of non-linear systems is the calculation of Lyapunov exponents, which are defined as [12]

$$\lambda_j \equiv \lim_{k\to\infty} \frac{1}{k} \ln \left\| a_j \left(\prod_{i=0}^{k} J^i \right) \right\|, \tag{15}$$

where $J^i \equiv \partial(r_{i+1}, \theta_{i+1})/\partial(r_i, \theta_i)$ is the Jacobian of the ith iteration of the mapping and $a_j(M)$ the jth eigenvalue of a matrix M. For a symplectic mapping it is known that $\sum_i \lambda_i = 0$ and thus for a bidimensional symplectic mapping $\lambda_1 = -\lambda_2$. So we have two possible cases: if $\lambda_1 = \lambda_2 = 0$ for a given trajectory of the system then this trajectory is regular; but, if $\|\lambda_1\| > 0$ then there is exponential divergence of nearby trajectories during the evolution and the trajectory is called chaotic. Of course we cannot perform exactly the infinite sum in (15) for numerical calculations, but the convergence of the maximum Lyapunov exponent occurs with good precision after just a few thousand iterations, both for regular and chaotic field lines (Fig. 8a).

Another analysis tool for systems with an angular coordinate is the safety factor, defined for a given trajectory as [22]

$$q \equiv \lim_{k\to\infty} \frac{2\pi k}{\sum_{j=0}^{k} (\theta_{j+1} - \theta_j)}, \tag{16}$$

which describes the medium inverse angular shift at each of the k iterations, each one with $\Delta\phi = 2\pi$. The trajectory can be classified in one of the three categories, according to the value of q: if q converges to an irrational number the trajectory is a regular closed torus along the angular coordinate; if q converges to a

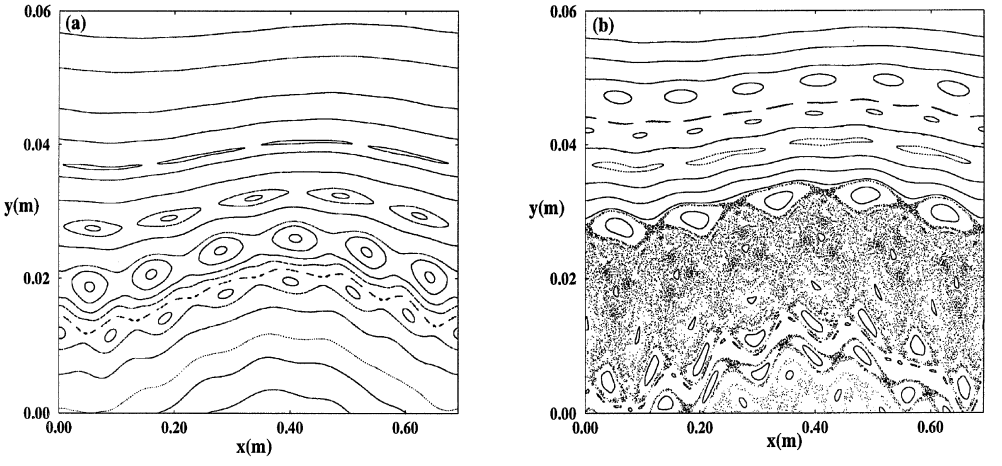

Fig. 6. Poincaré sections of the symplectic mapping with $m = 6$ and (a) $I = 200$ A, (b) $I = 800$ A in rectangular coordinates.

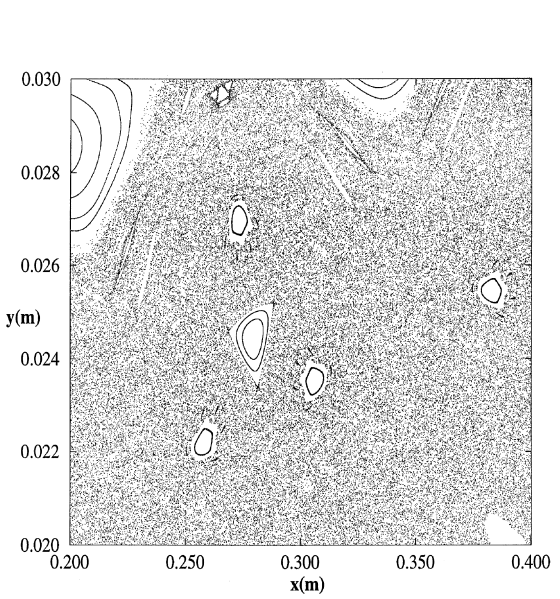

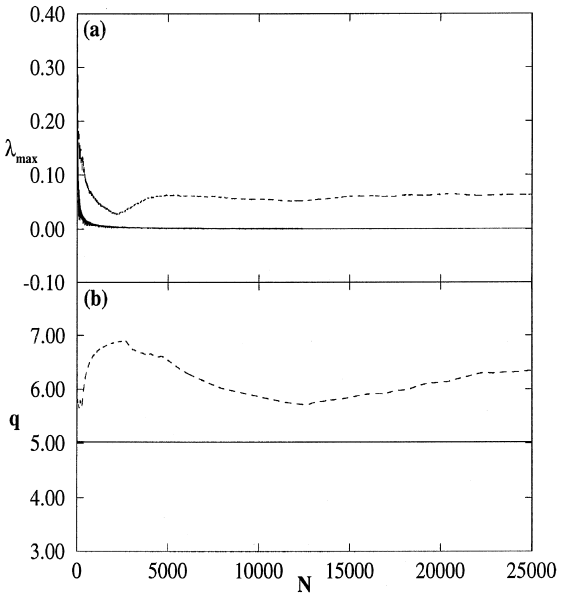

Fig. 7. Magnification of detail from the Poincaré plot of Fig. 6(b).

Fig. 8. Convergence curves of the: (a) Lyapunov exponents and (b) safety factors of a regular trajectory with $x_0 = 0.20m$ and $y_0 = 0.03m$ (solid lines) and a chaotic trajectory with $x_0 = 0.20m$ and $y_0 = 0.02m$ (dashed lines) for the symplectic mapping with $m = 6$ pairs of limiter current coils and $I = 800$ A.

rational number then the trajectory is either a resonant torus (for a magnetic limiter current $I = 0$) or belongs to a magnetic island chain (for $I > 0$); finally, if q does not converge to a real number, the trajectory is chaotic. In Fig. 8b we can see that for the regular trajectory q converges very quickly (as a matter of fact, we obtain $q = 5$, as the regular trajectory chosen is on the 5/1 magnetic island chain), but for the chaotic trajectory q does not converge at all.

With the aid of these two coefficients (the Lyapunov exponent and the safety factor) we are able to characterize completely the dynamical behavior of a given trajectory, and so we can analyze the relevant phenomena of the transition to chaos, such as island growth and overlapping, and island destruction, as we vary the initial conditions and parameters of our system.

5. Varying initial conditions and parameters

One of the most used methods in studying the dynamical behavior of non-linear systems is the plotting of characteristic coefficients (such as the Lyapunov exponents or the safety factors) for varying values of initial conditions or control parameters [23–26]. If we want to perform a more detailed analysis of a Poincaré section of the symplectic mapping for an intermediate current value (Fig. 9), where we have chaotic regions, magnetic islands, and a region of undestroyed magnetic tori, one of the possibilities is to calculate the Lyapunov exponents and the safety factors along a horizontal line across the Poincaré section, fixing the initial radial position y_0 (Fig. 10). We observe that the Lyapunov exponents of the chaotic regions have approximate medium value of $\langle\lambda\rangle \simeq 0.06$, and the transition from the null exponents in the island regions to the chaotic exponents is quite sudden, i.e., there are no less chaotic transition regions around the islands. Along this section we can observe the crossing of five magnetic islands, in whose interior the safety factors converge: three islands of the 7/1 chain ($q = 7.0$), one of the 8/1 chain ($q = 8.0$) and one of the 13/2 chain ($q = 6.5$); this last island is so small that it cannot be seen clearly in the Poincaré section (Fig. 9) but is clearly detected by the null Lyapunov exponents and the converging safety factors.

Another possibility is to analyze a vertical section of the Poincaré plot of Fig. 9, fixing the initial angular position x_0 (Fig. 11). In this case we can observe again that $\langle\lambda\rangle \simeq 0.06$ for all chaotic regions, which means

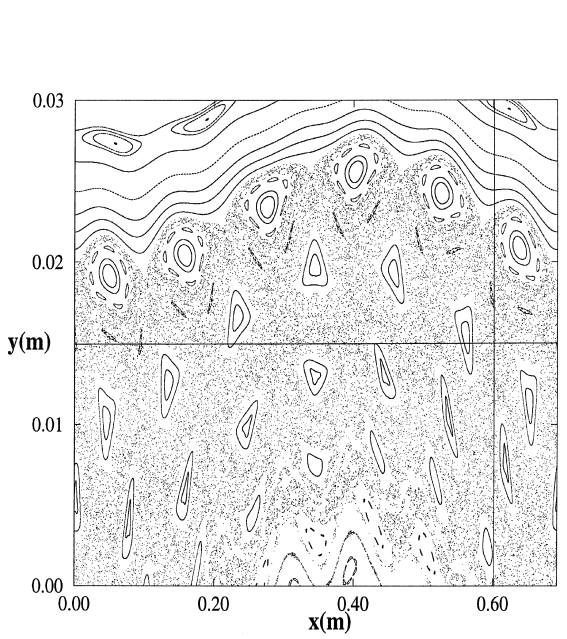

9

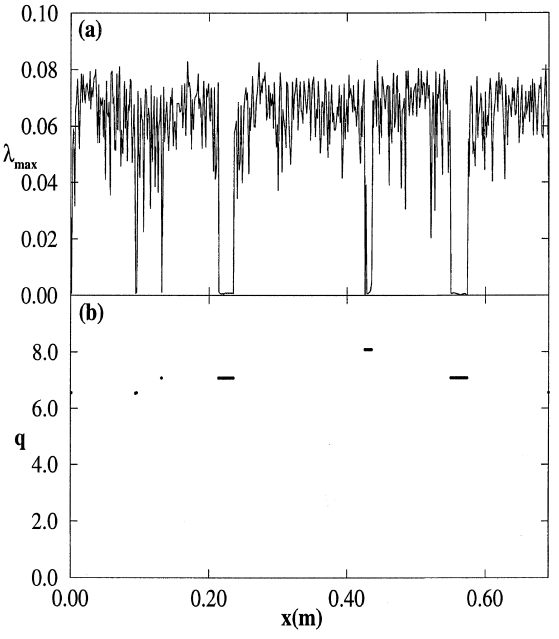

10

Fig. 9. Poincaré section of the symplectic mapping with $m = 7$ and $I = 400$ A.

Fig. 10. (a) Lyapunov exponents and (b) safety factors along the horizontal line in Fig. 9.

that even the chaotic regions close to the undestroyed tori are no less chaotic than the outer chaotic regions. As for the safety factors, they converge in three distinct regions: there is a large plateau with $q = 9.0$, corresponding to the crossing of the $9/1$ island chain, a very small region with $q = 6.5$, corresponding to the $13/2$ island chain again, and finally there is the region of the undestroyed magnetic field line tori where the safety factors assume the irrational values of each tori, which decrease as we increase y_0. As a matter of fact there are still very small regions of non-convergence of the safety factors in this structure, corresponding to the tiny chaotic layers around the separatrixes of the island chains which are beginning to grow of the resonant tori, but they can be observed only performing large magnifications.

An interesting way to analyze the growing of the magnetic island chains and the onset of chaos, as we increase the limiter current, is to plot the value of the maximum Lyapunov exponent for varying values of the initial radial position y_0 and the limiter current I for a fixed angular position x_0 (Fig. 12). In this kind of plot we can observe the appearance of the first thin chaotic layers at about $I \simeq 100$ A, which grow and join with others to form quite large chaotic regions as we increase the limiter current. Although this increase of chaotic field lines is very large at first, for higher currents ($I \simeq 500$ A) this growing stops because the growing of the inner magnetic surfaces of the island chains and the destruction of the outer ones counterbalance each other. So we can see that analytical predictions for the growth width of magnetic island chains, such as the square-root rule [8] are valid only for very low currents.

If we enlarge a part of this kind of plot (Fig. 13) we can see that the structure of the boundary between chaotic and regular regions is quite irregular. There are light gray "tongues" entering the borders of the dark chaotic regions, corresponding to secondary island chains which move as we increase the limiter current and are finally destroyed by the growing chaotic region. As each magnetic island has smaller secondary islands, and these islands have other even smaller secondary islands themselves, and so on, the boundary between the regular and chaotic regions is indeed fractal.

6. Conclusions

In this work we introduced a symplectic bidimensional mapping in order to describe the Poincaré section of the magnetic field lines in a tokamak chamber under the action of an ergodic limiter. We showed that the

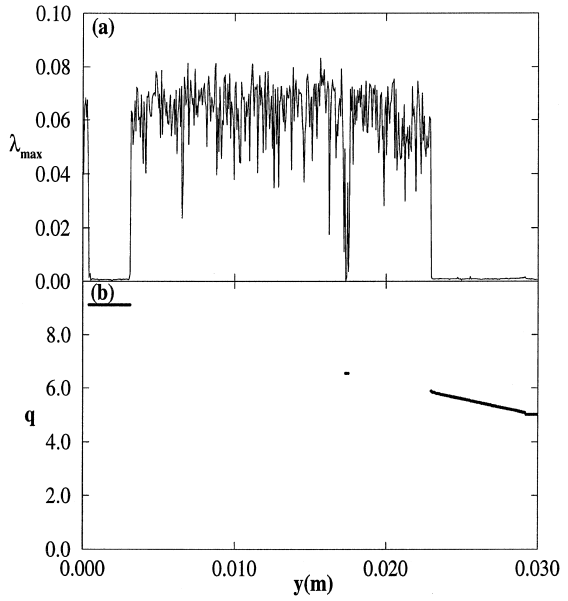

11

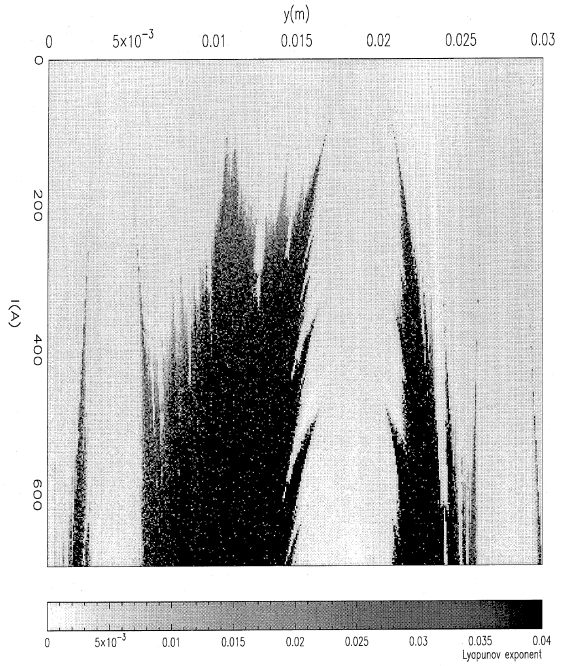

12

Fig. 11. (a) Lyapunov exponents and (b) safety factors along the vertical line in Fig. 9.

Fig. 12. Lyapunov exponents with $m = 6$ and $x_0 = 0.05m$.

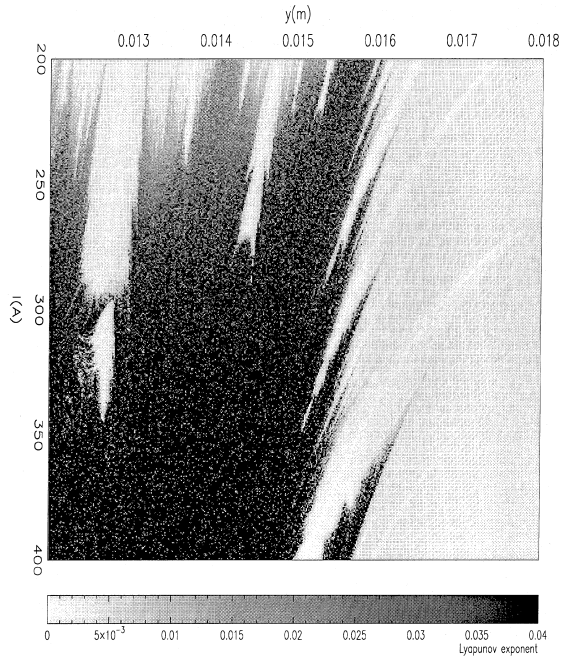

Fig. 13. Magnification of detail of Fig. 12.

symplecticity of the mapping is very important in order to study the chaotic dynamics at the plasma edge, at high limiter currents. In fact, these dynamics are much modified, as a consequence of combining the symplecticity condition, required for precise computation, and the realistic poloidal asymmetry of the

unperturbed field. Specially for high current limiters, not only new island chains are predicted by our mapping, but also a more pronunciated poloidal asymmetry is observed. Thus, the influence of an ergodic limiter on the plasma border can be more accurately described by this mapping which enlarges the possibility of the ergodic limiter dynamical analysis, in comparison with previous symplectic mappings that neglected toroidal corrections [13,14,27] or these that took into account these corrections but lacked the symplecticity condition [8].

Safety factors and Lyapunov exponents were calculated, varying the initial conditions and the control parameters, and the structure of the parameter plane showed very clearly the onset of chaos by the process of growing and destruction of secondary magnetic islands and a fractal boundary separating regular and chaotic regions [17]. It also revealed that at higher limiter currents the chaotic region at the plasma border does not grow very much, but remains, approximately, at the same size.

Finally it is important to emphasize that our model allows the introduction of an arbitrary poloidal magnetic field profile. Therefore it is suitable for numerical simulations of future interest, such as the research concerning non-monotonic profiles [28], whose experimental importance has been discussed [29,30], and the control of plasma-edge turbulence [3,7].

Acknowledgements

The authors would like to thank Dr. C. Ferro-Fontan (Universidad de Buenos Aires, Argentina) and Dr. R.L. Vaina (Universidade Federal do Paraná) for the useful discussions. This work was partially supported by FAPESP and CNPq (Brazilian Government Agencies).

References

[1] Wooton AJ, et al. Fluctuations and anomalous transport in tokamaks. Phys Fluids B 1990;2:2879.
[2] Wagner F, Stroh U. Transport in toroidal devices – the experimentalist's view. Plasma Phys Control Fusion 1993;35:1321.
[3] McCool S, et al. Electron thermal confinement studies with applied resonant fields on TEXT. Nucl Fusion 1989;29:547.
[4] Punjabi A, Verma A, Boozer A. Stochastic broadening of the separatrix of a tokamak divertor. Phys Rev Lett 1992;69:3322.
[5] Karger F, Lackner K. Resonant helical divertor. Phys Lett A 1977;61:385.
[6] Engelhardt W, Feneberg W. Influence of an ergodic magnetic limiter on the impurity content in a tokamak. J Nucl Mater 1978;76/77:518.
[7] Grosman A, et al. Radiactive layer control experiments with an ergodized zone in tore-supra. J Nucl Mater 1995;220/222:188.
[8] Caldas IL, Pereira JM, Ullmann K, Viana RL. Magnetic field line mappings for a tokamak with ergodic limiters. Chaos, Solitons & Fractals 1996;7:991.
[9] Ott E. Dynamical systems. Cambridge: Cambridge University press, 1993.
[10] Yorke JA, Alligood K, Sauer T. Chaos: An introduction to dynamical systems. New York: Springer, 1996.
[11] Habib S, Ryne RD. Symplectic calculation of Lyapunov exponents. Phys Rev Lett 1995;74:70.
[12] Schuster HG. Deterministic choas. Heidelberg: Physica-Verlag, 1984.
[13] Martin TJ, Taylor JB. Ergodic behavior in a magnetic limiter. Plasma Phys Control Fusion 1984;26:321.
[14] Viana RL, Caldas IL. Peripheral stochasticity in tokamak with an ergodic magnetic limiter. Z Naturforsch 1992;47:941.
[15] Regianni N, Sakanaka PH. The effect of the magnetic limiter current on the peripheral chaotic region of a tokamak. Plasma Phys Control Fusion 1994;36:513.
[16] Cary JR, Littlejohn RG. Noncanonical hamiltonian mechanics and its applications to magnetic field line flow. Ann Phys 1983;151:1.
[17] Lichtenberg AL, Lieberman MA. Regular and chaotic motion. 2nd ed. New York: Springer, 1992.
[18] Kucinski MY, Caldas IL, Monteiro LHA, Okano V. Toroidal plasma equilibrium with arbitrary current distribution. J Plasma Phys 1990;44:303.
[19] Nascimento IC, Caldas IL, Galvão RMO. Tokamak research at University of São Paulo. J Fusion Energy 1994;12:529.
[20] Almeida AMO. On the symplectically invariant variational principle and generating functions. Proc Royal Soc London A 1990;431:403.
[21] Hazeltine HD, Meiss JD. Plasma confinement. New York: Addison Wesley, 1992.
[22] Carreras B, Hicks HR, Waddell BV. Tearing-mode activity for hollow current profiles. Nucl Fusion 1979;19:583.
[23] Baptista MS, Caldas IL. Dynamics of the kicked logistic map. Chaos, Solitons & Fractals 1996;7:991.
[24] Ullmann K, Caldas IL. Transitions in the parameter space of a periodically forced dissipative system. Chaos, Solitons & Fractals 1996;7:1913.
[25] Rössler J, Kiwi M, Hess B, Markus M. Modulated non-linear processes and a novel mechanism to induce chaos. Phys Rev A 1989;39:5954.

[26] Gallas JAC. Structure of the parameter space of the Hénon map. Phys Rev Lett 1993;70:2714.
[27] Viana RL, Vasconcelos DB. Field-line stochasticity in tokamak with an ergodic magnetic limiter. Dynamics Stability Systems 1997;12:75.
[28] Oda GA, Caldas IL. Dimerized island chains in tokamaks. Chaos, Solitons & Fractals 1995;5:15.
[29] Leviton FM, et al. Improved confinement with reversed magnetic shear in TFTR. Phys Rev Lett 1995;75:4417.
[30] Strait EJ, et al. Enhanced confinement and stability in DIII-D discharges with reversed magnetic shear. Phys Rev Lett 1995;75:4421.